
HAMAMATSU PRESENTS
ANALYTICAL TALKS
WATCH NOW

LASER & PHOTONICS REVIEWS
www.lpr-journal.org

Diode-Pumped Laser Operation of Tb^{3+}:$LiLuF_4$ in the Green and Yellow Spectral Range

Elena Castellano-Hernández, Sascha Kalusniak, Philip W. Metz, and Christian Kränkel*

Here, a diode-pumped laser based on trivalent terbium (Tb^{3+}) as the active ion is reported. Optical pumping of a Tb^{3+}-doped lithium-lutetium-fluoride ($LiLuF_4$) crystal with up to 200 mW from a diode laser emitting at a wavelength of 488.2 nm enables continuous-wave lasing directly in the green and in the yellow. At an emission wavelength of 542 nm, the laser reaches an output power of up to 43.8 mW with a high slope efficiency of 52% with respect to the absorbed pump power. The yellow laser at 587 nm exhibits a slope efficiency of 22% and the output power of 13.8 mW is only limited by the available pump power. Laser thresholds as low as 14 and 27 mW of absorbed pump power are observed for the green and yellow, respectively. The investigations toward further optimization of the laser performance reveal that highly Tb^{3+}-doped materials are suitable for compact, efficient, and affordable diode-pumped solid-state lasers with direct emission in the visible spectral range. These results are of high relevance, as in particular for the yellow spectral range such systems are currently not available.

1. Introduction

Well-defined laser emission in the yellow range is required by a wide variety of applications in science, medicine, and technology. In science, yellow lasers are used for excitation of the D-line of absorption of sodium at 589 nm to generate artificial laser guide stars in astronomy.[1] In addition, laser emission at this wavelength is also required for sodium detection in spectroscopy and industry.[2] In medicine, yellow laser emission has the highest ratio of oxyhemoglobin absorption versus melanin absorption, reducing the laser power needed for macular photocoagulation treatments in a 30–40% in comparison with green lasers and thus decreasing the risk of retinal damage.[3] Yellow lasers have also proven their advantageous potential in skin therapies, such as treatment of vascular lesions, among others.[4]

Despite the rapid progress in laser research in the past nearly 60 years, up to now there is no convincing simple and easy to handle solution to generate continuous-wave (cw) laser emission in the yellow spectral range. The most straightforward approach to generate laser emission relies on electrically pumped semiconductor materials. However, the range of available direct emission wavelengths from semiconductor lasers exhibits a large gap in the visible range from the green to the orange spectral region (see **Figure 1**). Despite various approaches and ongoing research activities in this field,[5–10] the output power of experimental stage laser diodes in the yellow–orange spectral range is limited to mW power levels, mostly operated in pulsed regime with very low efficiencies. Laser diodes with emission in the green do exist, however, their efficiency and output power drastically decrease for wavelengths beyond 532 nm.

In fact, there are alternatives for visible lasers: dye lasers, in particular based on Rhodamine 6G, can provide kW pulsed average power, for example, in the yellow[18] but such flash lamp pumped systems are not suited for cw operation. Dye lasers in cw are limited to few watts of output power and dye degradation restricts the operating capacity at these power levels to only a few 100 hours per liter of dye solution.[19,20] Furthermore, the toxic and carcinogenic nature of most dyes requires precaution during their exchange. The pump power conversion efficiency of cw dye lasers can be as high as 30%, but—though diode pumping seems feasible[21]—in most cases, the pump source itself is a complicated frequency doubled neodymium (Nd^{3+}) laser system. Finally, even sophisticated solid-state dye laser concepts are limited to few 10 mW of cw output power due to dye degradation.[22]

For these reasons, many dye lasers were replaced by upcoming nonlinear laser systems with visible emission in the past years. Intracavity frequency doubling enables highly efficient green emission,[23] but suitable fundamental sources around 1.2 μm for frequency doubling into the yellow range are rare. Hence, the existing frequency doubled yellow lasers are still fairly complex or limited in cw scaling potential.[24–26] Other nonlinear approaches such as sum frequency mixing,[27] optical parametric oscillators

E. Castellano-Hernández, Dr. S. Kalusniak, Dr. C. Kränkel
Center for Laser Materials
Leibniz-Institut für Kristallzüchtung (IKZ)
Max-Born-Str. 2, 12489 Berlin, Germany
E-mail: elena.castellano@ikz-berlin.de
Dr. P. W. Metz
Institut für Laser-Physik
Universität Hamburg
Luruper Chaussee 149, 22761 Hamburg, Germany

The ORCID identification number(s) for the author(s) of this article can be found under https://doi.org/10.1002/lpor.201900229

DOI: 10.1002/lpor.201900229

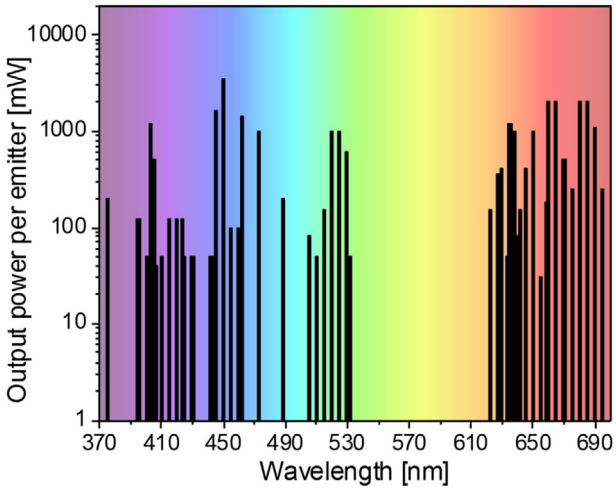

Figure 1. Output power of single emitter laser diodes provided by different suppliers versus emission wavelength.[11–17]

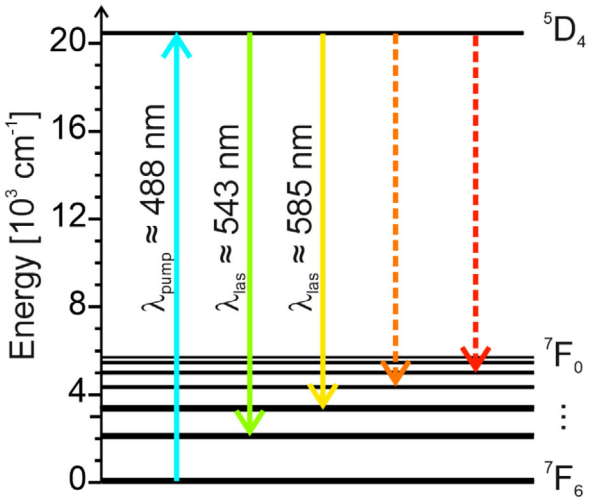

Figure 2. Energy level diagram of Tb^{3+} with relevant laser transitions (solid arrows). Dashed arrows correspond to transitions in the orange and red spectral range, where laser operation is not expected.

(OPOs),[28] or Raman shifted fundamental sources[29] increase the level of complexity even further.

Given the absence of semiconductor materials suitable for laser diodes in the 550–600 nm spectral range, diode-pumped solid-state lasers with direct emission in the green to yellow spectral range represent the most simple and scalable solution to address these wavelengths. Since the advent of blue laser diodes as useful pump sources, a large variety of direct visibly emitting diode-pumped lasers has been realized.[30,31] However, among these, only a few emit in yellow.

In particular, laser materials doped with trivalent praseodymium (Pr^{3+}) enable remarkably efficient laser operation at several wavelengths within the green to orange gap in the semiconductor emission range. Up to 60% of slope efficiency was demonstrated, for example, at wavelengths of 546 nm in the green and 607 nm in the orange spectral range under blue diode pumping.[31] However, Pr^{3+} ions do not allow for laser operation at wavelengths between 550 and 600 nm due to ground state absorption losses into the $^1D_2$-multiplet. Thus, trivalent dysprosium (Dy^{3+}),[32] samarium (Sm^{3+}),[33] and Tb^{3+}[34,35] are the only known laser active ions suitable for direct yellow emission. Among these, Sm^{3+} and Tb^{3+} were previously only pumped by complex frequency doubled optically pumped semiconductor lasers (2ω-OPSL). The only previous diode-pumped yellow emitting solid-state laser based on Dy^{3+}:$LiLuF_4$ (LLF) possessed a high laser threshold in excess of 300 mW and a slope efficiency of 13.4% with a maximum cw output power of 55 mW at 574 nm. This insufficient performance is owed to the properties of the $^6H_{13/2}$ terminal level of the respective Dy^{3+} laser transition, which, even utilizing Tb^{3+}-codoping for depopulation, exhibits too long a lifetime.[32] In contrast, yellow emitting Tb^{3+}-doped laser materials exhibit an order of magnitude lower laser thresholds and slope efficiencies in excess of 25% under pumping with a 2ω-OPSL at 486 nm.[34,35]

Here, we present what we believe to be the simplest and most efficient direct yellow emitting solid-state laser up to now. The first diode-pumped Tb^{3+}:LLF laser exhibits a slope efficiency of 22% at a wavelength of 587 nm in the yellow spectral range under pumping with a diode laser emitting up to 200 mW at 488 nm. An even better performance was obtained at 542 nm in the green with a slope efficiency of 53%. The whole setup utilizes no nonlinear conversion processes and power scaling is only limited by the currently available pump power.

2. Active Gain Media and Experimental Setup

The energy level splitting of Tb^{3+} and the corresponding intraconfigurational 4f–4f transitions from the $^5D_4$ level to the ^7F manifold allow for light emission in the visible range (see **Figure 2**). For a long time, this emission was not thought to be useful for laser operation due to the low energetic position of the $4f^75d^1$ energy levels in Tb^{3+} and the resulting possibility for detrimental excited state absorption (ESA) from 4f into 5d energy levels.[36] Recent work revealed that efficient laser operation under 2ω-OPSL pumping is indeed possible in the green and yellow spectral range, which is explained by a strongly forbidden double spin–flip transition from the excited state $^5D_4$ of the 4f configuration into the lowest energy multiplet ^9D of the 5d configuration. This spin–flip heavily reduces the probability for corresponding ESA transitions in the visible.[37] However, detrimental 4f–4f ESA processes still prohibit laser operation in the orange and in the red in Tb^{3+}:LLF.[34,35,38] To further avoid ESA from the excited state $^5D_4$ into higher and only singly spin-forbidden, energy levels of the 5d configuration, it is still crucial to choose a host material with a large energy gap between the 4f energy ground state and the next higher levels of the 5d configuration ^7D.[39] The low crystal field strength of fluorides compared to other laser host materials,[36] fulfills this requirement, and makes them suitable host materials for green and yellow Tb^{3+} lasers.

For the laser experiments accomplished in this report, we utilized a Tb^{3+}:LLF sample with a length of 18.5 mm. The Tb^{3+} ion concentration of 28 at% in the crystal was determined by microprobe analysis. The a-cut orientation of the tetragonal crystal structure gives access to both, π- and σ-polarization of the sample. The plane-parallel polished faces provide a clear aperture of

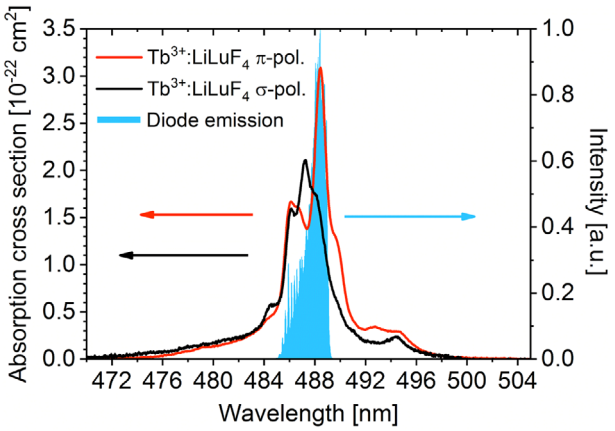

Figure 3. Polarization dependent absorption cross sections of Tb^{3+}:LLF (black and red lines) and emission of the diode laser pump source (blue area).

≈5 mm. The sample orientation was verified by Laue and pole-figure measurements with an X-ray diffraction system (GE Inspection Tech.).

An indium-gallium-nitride (InGaN)-based diode laser (iBeam Smart, Toptica Photonics) with an emission wavelength of 488.2 nm with a full width at half maximum (FWHM) emission bandwidth of 1.3 nm and a maximum output power of 200 mW served as a pump source for the laser experiments. Its emission wavelength was chosen to match the highest peak of the $^7F_6 \rightarrow {}^5D_4$ ground state absorption of Tb^{3+} in π-polarization into the upper laser level (see **Figure 3**). The absorption cross sections shown in Figure 3 were calculated from absorption measurements performed in the laser sample by a Lambda 1050 spectrophotometer (Perkin Elmer) with a spectral resolution of 0.15 nm. The diode emission exhibits a divergence of <1 mrad and a beam quality of $M^2 < 1.2$ at an emitted beam diameter of 1 mm × 0.97 mm ($1/e^2$). In addition, the laser stability exhibits a standard deviation of 0.2%. These features qualify the diode laser as a suitable pump source for high efficient laser performance. It should be noted that the emitted beam diameter is smaller than that in our previous experiments using a 2ω-OPSL as a pump source, resulting in different optimum focusing conditions.[34]

Figure 4 shows a schematic of the laser setup. A Faraday isolator (Qioptiq Photonics) placed after the diode output prevents potentially harmful optical feedback into the laser diode. In order to avoid wavelength drift of the diode emission with current, the diode was operated at maximum power at all times. To adjust the incident pump power onto the crystal, a set of $\lambda/2$-plate and polarizing beam splitter was placed after the Faraday isolator. For focusing the pump light on the crystal, different plano-convex lenses were tested. The best results were obtained with focal lengths of 150 or 100 mm for green or yellow laser operation, respectively, focused the pump beam on the crystal, which was placed in a passive copper heat sink. The resulting focal diameters in the center of the crystal were 165 µm for the green and 102 µm for the yellow laser, and increased to 167 and 111 µm, respectively, at the crystal surface. Our simulations showed that with these pump beam waists, a close to perfect match with the fundamental TEM_{00} laser mode can be achieved in the nearly concentric resonator design. Again, it should be noted that due to the smaller diameter of the diode beam, the pump beam is less divergent in the crystal as compared to the previous results under 2ω-OPSL pumping.[34] The stronger focus for the yellow laser turned out to be advantageous for the achievable output power in view of the moderately higher thresholds at this transition. In both cases, the single pass absorption efficiency of the crystal amounted to ≈77% of the incident beam. The simple nearly concentric laser cavity consisted of two mirrors with radii of curvature of 100 mm separated by a distance of ≈200 mm. The pump mirrors (PM) had high transparency for the pump wavelength, while they were highly reflective (HR) for the respective laser wavelength. We utilized different output coupler mirrors (OCM) with transmissions of up to 3.3% for the laser wavelength. To separate the laser beam from the residual pump light, we used a dichroic mirror (DMLP505 Thorlabs) for the green and an absorptive glass filter (Schott OG515) for the yellow laser. The dichroic mirror, placed at an angle of 45° with respect to the incident beam, has a transmission of 98.8% for 542 nm and 0.8% for 488 nm. The glass filter has a transmission of 90.9% for 587 nm and ≈0% for 488 nm.

3. Results and Discussion

3.1. Diode-Pumped Green Laser Emission

The green laser emission corresponds to the Tb^{3+} transition $^5D_4 \rightarrow {}^7F_5$ (see Figure 2). This transition at a wavelength of 542 nm has an emission cross-section of 1.0×10^{-21} cm^2 for π-polarization and 1.3×10^{-21} cm^2 for σ-polarization. A second peak at 544.1 nm exhibits emission cross-sections of 0.8×10^{-21} cm^2 for π-polarization and 1.6×10^{-21} cm^2 for σ-polarization.[34] The laser experiments were performed using several OCMs with transmissions between <0.2% (HR) and 2.6% (see **Figure 5** (left)). The laser operates at a center emission wavelength of 544.1 nm for the two OCMs with the lowest transmission, HR and 0.4%, and at 542.4 nm for the two OCM with the higher transmissions, 1.3% and 2.6%. This variation in the emission wavelength is attributed to the detailed transmission characteristics of the mirror coatings rather than to the change in population

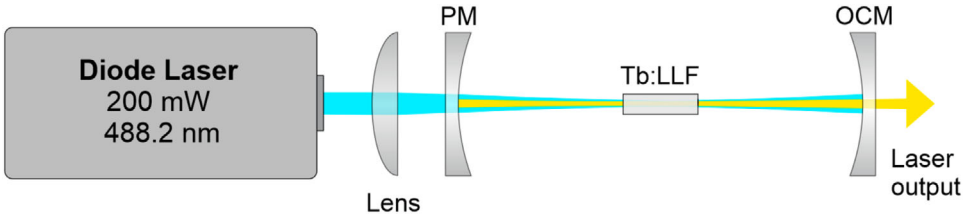

Figure 4. Schematic of the diode-pumped Tb:LLF laser cavity.

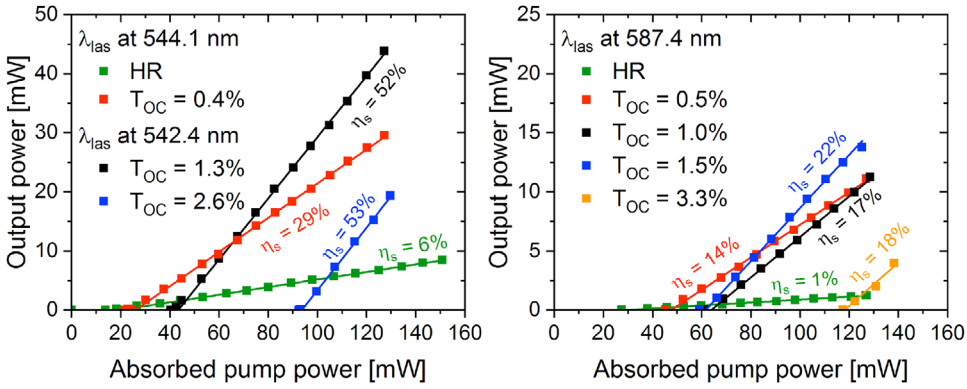

Figure 5. Laser characteristics of an 18.5 mm long diode-pumped Tb^{3+} (28 at%):LLF crystal for different output coupler transmissions T_{oc} and different laser emission wavelengths λ_{las}. (Left) Characteristics for laser emission in the green spectral range and (right) in the yellow spectral range. Note the factor of two between the scaling of both y-axes.

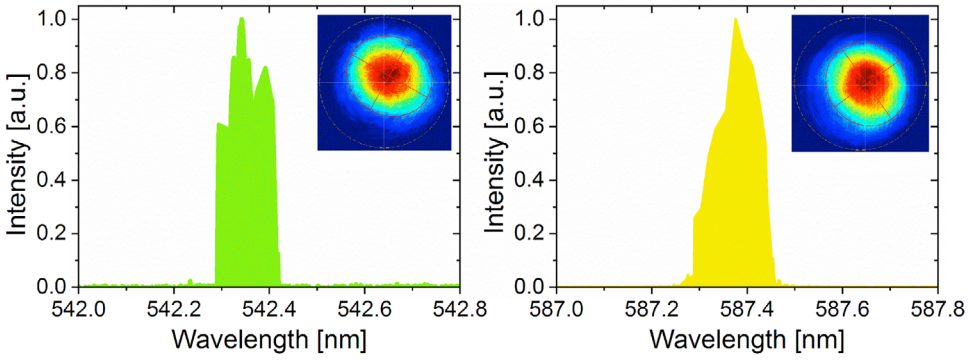

Figure 6. Laser emission spectra for (left) green emission centered at 542.4 nm at maximum output power with an output coupler transmission of 1.3%; and (right) yellow emission centered at 587.4 nm at maximum output power with an output coupler transmission of 1.5%. Insets: Beam profiles of the lasers under the same conditions.

of the respective energy levels. For the HR and the 0.4% OCM, the transmission between 542.4 and 544.1 nm is fairly plain and the highest peak of emission of Tb^{3+}:LLF is at 544 nm. However, for the 1.3% and the 2.6% OCM, the transmission of the mirrors increases with wavelength, making the conditions more favorable for the laser to operate at the emission peak at 542 nm. As expected from the emission spectra,[34] in all cases the laser emission was found to be polarized perpendicular to the *c*-axis of the crystal. Even though Tb^{3+}:LLF is reported to support laser operation at output coupler transmissions as high as 11.9%,[35] the maximum diode laser emission of 200 mW did not allow to reach the laser threshold for OCM transmissions higher than 2.6%. This transmission yielded the highest slope efficiency of 53%, but the maximum output power was limited to 19.2 mW by the available pump power. At a similar slope efficiency of 52%, the highest output power of 44 mW was obtained with the OCM with a transmission of 1.3% at a corresponding absorbed pump power of 127 mW. The resulting optical-to-optical efficiency amounted to 34.5% and the laser threshold was as low as 40 mW. Stability measurements of the laser output showed a standard deviation of 2.5% under these conditions. The minimum laser threshold achieved with the HR mirror was as low as 14 mW of absorbed pump power. The laser emission spectrum at maximum output power shown in **Figure 6** (left) was measured by an optical spectrum analyzer (AQ6374, Yokogawa) with a spectral resolution below 0.05 nm. The FWHM of the emission is around 0.1 nm. The emission in the green spectral range is centered at 542.4 nm. The inset shows the output beam profile at maximum power, recorded by a CinCam-CMOS-1202 (Cinogy Tech.) camera, revealing Gaussian power distribution in fundamental transverse electromagnetic mode TEM_{00}.

3.2. Diode-Pumped Yellow Laser Emission

The yellow laser emission of Tb^{3+} ions corresponds to the transition $^5D_4 \rightarrow {}^7F_4$ (see Figure 2) located at a wavelength of 587.4 nm. This transition exhibits a peak emission cross-section of 1.1×10^{-21} cm^2 for π-polarization and the peak cross section of 0.47×10^{-21} cm^2 for σ-polarization is found at 582 nm.[34] The laser experiments were performed with several OCMs with transmissions between <0.2% (HR) and 3.3% (see Figure 5 (right)). The laser operates around 587.4 nm for all OCMs. As in the case of green emission, the maximum pump power of 200 mW did not allow for laser operation with higher output coupler transmissions. The laser emission was always polarized parallel to the *c*-axis of the crystal.

The best performance of the yellow Tb^{3+}:LLF laser in terms of maximum output power and slope efficiency was obtained using the OCM with a transmission of 1.5%. The corresponding slope

efficiency was 22% and the maximum output power amounted to 13.8 mW at an absorbed pump power of 125.3 mW. The resulting optical-to-optical efficiency was 11.0% and the laser threshold reached at 59 mW of absorbed pump power. The laser emission spectrum and the beam profile can be found in Figure 6 (right). Stability measurements of the laser output yielded a standard deviation of 4.1% for this configuration. The lowest laser threshold of 27 mW was found for the HR mirror.

In addition, during the operation with the HR mirror, it was possible to force the laser to operate at a wavelength of 582.0 nm by cavity alignment. Under these conditions, the maximum output power was 0.6 mW with a slope efficiency of 1.6% and a laser threshold of 86 mW of absorbed pump power.

3.3. Discussion

The results of these experiments on diode pumping of a Tb^{3+} doped solid-state laser are comparable to those obtained previously under 2ω-OPSL-pumping as can be seen in **Figure 7** for the example of the green laser transition. In all cases including the yellow laser, the slope efficiencies and laser thresholds at comparable output coupler transmissions are very similar to the values obtained under 2ω-OPSL-pumping,[34] which is enabled by the good beam quality of the single emitter laser diode used here. Even though the best optical efficiencies that were obtained under 2ω-OPSL-pumping in the order of 38% are higher than the results of up to 25% presented here, it should be taken into account that the 2ω-OPSL itself is a diode-pumped frequency doubled laser with an internal efficiency below 25%. Therefore, the authentic optical-to-optical efficiency (and also the wall-plug efficiency) is much higher under diode pumping.

In addition, these results, and in particular the low pump threshold powers, give rise to the prediction that significant further scaling of the output power of diode-pumped Tb^{3+} lasers is feasible even with high-power multi-mode laser diodes with lower beam quality.

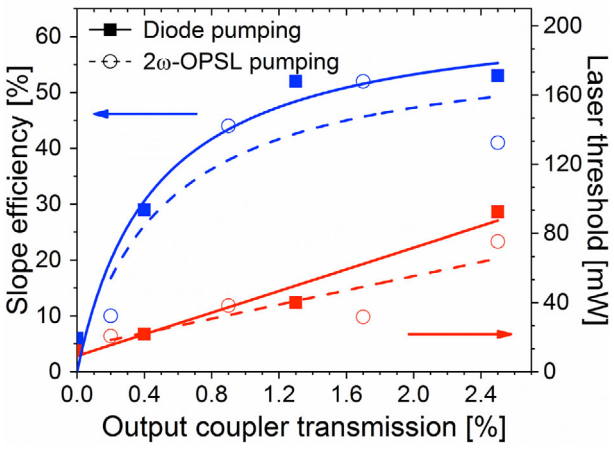

Figure 7. Comparison of laser performance of Tb^{3+} (28 at%):LLF under 2ω-OPSL and laser diode pumping in the green spectral range. Here, the respective fit curves (blue: Caird[40] (cf. Figure 8, same data for diode pumping), red: linear) mainly serve as a guide to the eye. It should be noted that different focusing conditions and crystal lengths were used during 2ω-OPSL pumping[34] (21.1 mm) and diode pumping (18.5 mm).

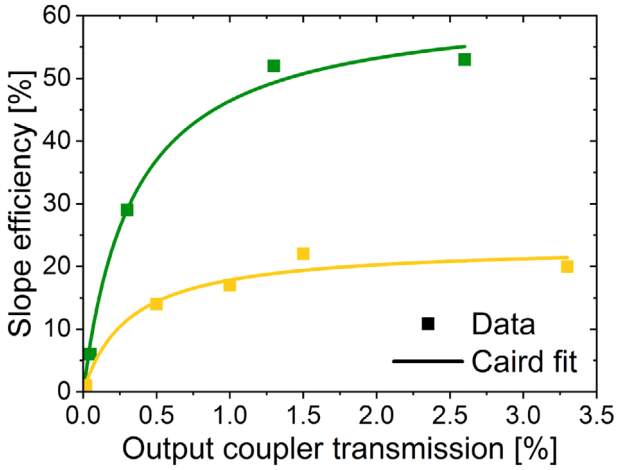

Figure 8. Slope efficiencies for different output coupler transmissions. The green dots correspond to laser emission at 542.4 and 544.1 nm, and the yellow dots to laser emission at 587.4 nm. The solid lines represent the respective Caird fits according to $\eta_s = \eta' \cdot T \cdot (T + L)^{-1}$,[40] where T is the output coupler transmission, L the cavity losses, and η' the internal slope efficiency.

In this context, it should be noted that the available efficiency is not limited by the spatial overlap between the pump and the laser mode, or the losses in the 18.5 mm long gain medium. **Figure 8** shows the laser slope efficiency versus the output coupler transmission for the green and yellow emission. The solid lines correspond to Caird fits,[40] yielding low cavity losses of 0.3% for both wavelengths. In a simple rate equation model, the slope efficiency η_{slope} of a laser is determined by the equation

$$\eta_{slope} \leq \eta_{Stokes} \cdot \eta_{overlap} \cdot \eta_{quantum} \cdot \eta_{resonator} \quad (1)$$

where the Stokes efficiency η_{Stokes} is the ratio of the laser and pump photon energies, $\eta_{overlap}$ is the mode overlap efficiency between the pump and the laser mode, the quantum efficiency $\eta_{quantum}$ is the ratio of laser transitions to all transitions from the upper laser level (i.e., including possible non-radiative or ESA transitions), and the resonator efficiency $\eta_{resonator}$ is the ratio of the output coupling losses to the total resonator losses.

The resulting internal slope efficiencies η' of 62% for the green emission and 23% for the yellow are clearly below the respective Stokes efficiencies of 90% and 83%. The deviation between the internal slope efficiency and the Stokes efficiency is much larger for the yellow laser, while - as mentioned above - the mode overlap is very similar for both lasers. Consequently, the ratio of the internal slope efficiencies depends only on the Stokes efficiency and the quantum efficiency. With the known values for the Stokes efficiency, the resulting ratio between the quantum efficiencies in the green and the yellow amount to 0.4. We attribute this lower quantum efficiency of the yellow Tb^{3+}:LLF laser to remaining 4f–4f ESA processes that do not fully prohibit laser operation but decrease the efficiency of this transition. We can nearly exclude ESA into 5d levels, as this would also affect the green laser with its even higher photon energies.

4. Outlook

Despite the high doping concentrations, the 18.5 mm long Tb^{3+}(28 at%):LLF sample exhibits a single pass absorption efficiency of only 77% even at the peak absorption wavelength. An increased absorption capability would enable shorter lengths of the active medium which could possibly increase the laser efficiency by an increased mode matching and enable real miniaturization of yellow-emitting diode-pumped solid-state lasers. Higher doping concentrations might be beneficial; however, they often come at the expense of detrimental interionic processes which quench the upper laser level lifetime by increasing non-radiative decay processes. To investigate the potential of Tb^{3+}:LLF in this respect, we measured the fluorescence lifetimes of LLF samples doped with different concentrations of Tb^{3+}. These measurements were performed by exciting the crystals at 488 nm with an optical parametric oscillator (VersaScan, GWU-Lasertechnik) emitting mJ-pulses of 5 ns duration at a repetition rate of 10 Hz. The fluorescence at 543 nm was detected behind a monochromator M Series II (Horiba) by an R5108 photomultiplier (Hamamatsu). The photomultiplier signal was recorded in an RTE1204 oscilloscope (Rohde & Schwarz).

The spin-forbidden character of the fluorescence transitions from the upper laser level $^5D_4$ into the ground state multiplets ^7F_J yields lifetimes in the order of few milliseconds. **Figure 9** depicts the fluorescence lifetime for four different Tb^{3+} concentrations in $LiLuF_4$ of 2%, 14%, 28%, and 100% ($LiTbF_4$). The concentrations were determined by microprobe analyses. The fluorescence lifetime of 4.8 ms remains unquenched even for concentrations as high as 28 at%. For the highest possible concentration of Tb^{3+} in this matrix, the stoichiometric crystal lithium-terbium-fluoride ($LiTbF_4$), the measured fluorescence lifetime of 2 ms still yields a radiative quantum efficiency of more than 40%, which is remarkably high for such a large active ion concentration. In addition, this reduction in the $LiTbF_4$ lifetime is potentially caused by rare-earth impurities, for example, Sm^{3+},[38] rather than by the Tb^{3+} ions themselves and could even be mitigated by the use of highly pure starting materials during the crystal growth process. Therefore, we believe that the investigation of Tb^{3+} concentrations between 40% and 75% could allow for further significant improvement of the laser performance, in particular when it comes to high power diode pumping. An improved performance could also be facilitated by the choice of a different host material: in particular the suggested 4f–4f ESA acceptor level for the yellow transition is expected to exhibit a narrow bandwidth typical for 4f energy levels and its position should slightly shift in different host crystals. In the absence of ESA, the laser performance of Tb^{3+} in the yellow should be similar to the results obtained in the green.

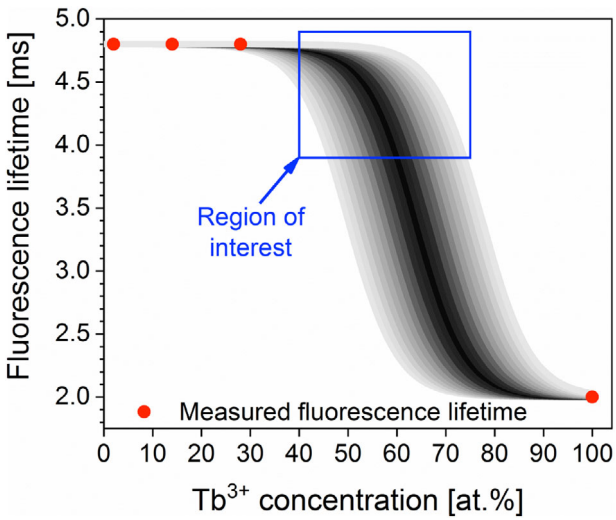

Figure 9. Measured fluorescence lifetime of the excited state $^5D_4$ in Tb^{3+}:LLF for different Tb^{3+} concentrations in the crystal (red dots). The gray shaded regions show possible tendencies for the lifetime quenching of Tb^{3+}:LLF toward higher doping concentrations.

It should also be noted that the long upper state lifetime of Tb^{3+} gives rise to high storage energies, which may be beneficial for high pulse energies in future experiments on Q-switched laser operation using visible saturable absorber materials.[41]

Furthermore, tunable laser operation over several nanometers has been demonstrated for the green spectral range in Tb^{3+}-doped laser materials,[38] and our preliminary results on laser operation at 582 nm also render it possible to achieve wavelength tuning in the yellow spectral range and to improve the performance at 582 nm by the use of optimized mirror coatings.

5. Conclusion

We demonstrated diode-pumped laser operation of a Tb^{3+}-doped material. The simple approach of this work does not involve any nonlinear wavelength conversion process, neither in the pump source nor in the laser cavity. The laser emission at 542.4 nm in the green spectral range exhibits high slope efficiency in excess of 50%, and, in the yellow at 587.4 nm, the maximum slope efficiency amounts to 22%. In all cases, the output power was only limited by the available pump power. Therefore, the future progress in cyan-blue emitting diode lasers at 488 nm should enable further improvement of the laser performance, which will be supported by the use of higher doping concentrations possible due to the late onset of concentration quenching of the emitting level lifetime demonstrated here.

Our diode-pumped visibly emitting solid-state lasers exhibit low laser thresholds below 30 mW of absorbed pump power. Hence, these systems are a convenient, efficient, and possible to miniaturize alternative to nonlinear systems, in particular in the low power range, where nonlinear conversion efficiencies are intrinsically lower. While wavelength tuning in the green spectral range has previously been demonstrated with Tb^{3+} doped materials, our results also indicate the tuning capacity in the yellow spectral range, which will be confirmed in future experiments.

Acknowledgements

The authors thank Albert Kwasniewski from the X-ray group at IKZ for orientating the Tb^{3+}:LLF crystal and the crystal processing group at IKZ for support in sample preparation. This work was funded by the German Bundesministerium für Bildung und Forschung (BMBF) (13N14192).

Conflict of Interest

The authors declare no conflict of interest.

Keywords

diode-pumping, solid-state lasers, terbium, visible lasers, yellow lasers

Received: July 11, 2019
Revised: November 25, 2019
Published online: January 15, 2020

[1] M. Duering, V. Kolev, B. Luther-Davies, *Opt. Express* **2009**, *17*, 437.
[2] P. Juncar, J. Pinard, J. Hamon, A. Chartier, *Metrologia* **1981**, *17*, 77.
[3] M. A. Mainster, *Ophthalmology* **1986**, *93*, 952.
[4] T. Karppinen, E. Kantola, A. Karppinen, A. Rantamäki, H. Kautiainen, S. Mordon, M. Guina, *Lasers Surg. Med.* **2019**, *51*, 223.
[5] N. N. Ledentsov, V. A. Shchukin, Y. M. Shernyakov, M. M. Kulagina, A. S. Payusov, N. Y. Gordeev, M. V. Maximov, A. E. Zhukov, T. Denneulin, N. Cherkashin, *Opt. Express* **2018**, *26*, 13985.
[6] T. Tanaka, H. Yanagisawa, M. Takimoto, S. Minagawa, *Electron. Lett.* **1993**, *29*, 1864.
[7] J. Feng, R. Akimoto, *Appl. Phys. Express* **2016**, *9*, 012101.
[8] C. J. Nuese, A. G. Sigai, J. J. Gannon, *Appl. Phys. Lett.* **1972**, *20*, 431.
[9] D. P. Bour, D. W. Treat, K. J. Beernink, B. S. Krusor, R. S. Geels, D. F. Welch, *IEEE Photonics Technol. Lett.* **1994**, *6*, 128.
[10] L. Toikkanen, A. Härkönen, J. Lyytikäinen, T. Leinonen, A. Laakso, A. Tukiainen, J. Viheriälä, M. Bister, M. Guina, *IEEE Photonics Technol. Lett.* **2014**, *26*, 384.
[11] Toptica Photonics laser diodes, https://www.toptica.com/products/wavemeters-laser-diodes/laser-diodes/ (accessed: **2019**) (accessed: April 2019).
[12] Nichia laser diodes, http://www.nichia.co.jp/en/product/laser.html (accessed: April 2019).
[13] Frankfurt Laser Company laser diodes, https://www.frlaserco.com/Laser-Diodes (accessed: April 2019).
[14] Laser Diode Source homepage, https://www.laserdiodesource.com/ (accessed: April 2019).
[15] OSRAM product portfolio, https://www.osram.com/os/products/index.jsp (accessed: April 2019).
[16] Thorlabs visible laser diodes, https://www.thorlabs.de/newgrouppage9.cfm?objectgroup_id=7 (accessed: April 2019).
[17] Laser Components CW Laser Diodes, https://www.lasercomponents.com/de-en/product/cw-laser-diodes-blue/ (accessed: April 2019).
[18] D. E. Klimek, H. R. Aldag, *Proc. SPIE* **1993**, *1871*, 72.
[19] B. Wellegehausen, L. Laepple, H. Welling, *Appl. Phys.* **1975**, *6*, 335.
[20] Sirah Rhodamine 6G laser, http://www.sirah.com/dyes-accessories/laser-dyes-532-nm/rhodamine-6g-new (accessed: **2019**) (accessed: April 2019).
[21] O. A. Burdukova, M. V. Gorbunkov, V. A. Petukhov, M. A. Semenov, *Laser Phys. Lett.* **2016**, *13*, 105004.
[22] R. Bornemann, U. Lemmer, E. Thiel, *Opt. Lett.* **2006**, *31*, 1669.
[23] L. McDonagh, R. Wallenstein, *Opt. Lett.* **2007**, *32*, 802.
[24] M. Guina, A. Rantamäki, A. Härkönen, *J. Phys. D: Appl. Phys.* **2017**, *50*, 383001.
[25] E. Kantola, T. Leinonen, S. Ranta, M. Tavast, M. Guina, *Opt. Express* **2014**, *22*, 6372.
[26] L. Taylor, Y. Feng, D. Bonaccini Calia, *Opt. Express* **2009**, *17*, 14687.
[27] C. A. Denman, P. D. Hillman, G. T. Moore, J. M. Telle, J. E. Preston, J. D. Drummond, R. Q. Fugate, presented at Advanced Solid-State Photonics (TOPS), Vienna, February **2005**, paper 698.
[28] U. Strößner, J.-P. Meyn, R. Wallenstein, P. Urenski, A. Arie, G. Rosenman, J. Mlynek, S. Schiller, A. Peters, *J. Opt. Soc. Am. B* **2002**, *19*, 1419.
[29] A. J. Lee, D. J. Spence, J. A. Piper, H. M. Pask, *Opt. Express* **2010**, *18*, 20013.
[30] C. Kränkel, D.-T. Marzahl, F. Moglia, G. Huber, P. W. Metz, *Laser Photonics Rev.* **2016**, *10*, 548.
[31] P. W. Metz, F. Reichert, F. Moglia, S. Müller, D.-T. Marzahl, C. Kränkel, G. Huber, *Opt. Lett.* **2014**, *39*, 3193.
[32] G. Bolognesi, D. Parisi, D. Calonico, G. A. Costanzo, F. Levi, P. W. Metz, C. Kränkel, G. Huber, M. Tonelli, *Opt. Lett.* **2014**, *39*, 6628.
[33] D.-T. Marzahl, P. W. Metz, C. Kränkel, G. Huber, *Opt. Express* **2015**, *23*, 21118.
[34] P. W. Metz, D.-T. Marzahl, A. Majid, C. Kränkel, G. Huber, *Laser Photonics Rev.* **2016**, *10*, 335.
[35] E. Castellano-Hernández, P. W. Metz, M. Demesh, C. Kränkel, *Opt. Lett.* **2018**, *43*, 4791.
[36] P. Dorenbos, *Phys. Rev. B* **2000**, *62*, 15640.
[37] P. W. Metz, C. Kränkel, G. Huber, presented at 6th EPS-QEOD Europhoton Conf., Neuchâtel, Switzerland, August **2014**.
[38] P. W. Metz, D.-T. Marzahl, G. Huber, C. Kränkel, *Opt. Express* **2017**, *25*, 5716.
[39] P. Dorenbos, A. H. Krumpel, E. van der Kolk, P. Boutinaud, M. Bettinelli, E. Cavalli, *Opt. Mater.* **2010**, *32*, 1681.
[40] J. A. Caird, S. A. Payne, P. R. Staber, A. J. Ramponi, L. L. Chase, W. F. Krupke, *IEEE J. Quantum Electron.* **1988**, *24*, 1077.
[41] M. Demesh, D. T. Marzahl, A. Yasukevich, V. Kisel, G. Huber, N. Kuleshov, C. Kränkel, *Opt. Lett.* **2017**, *42*, 4687.